Chemical Science

ROYAL SOCIETY OF CHEMISTRY

EDGE ARTICLE

View Article Online
View Journal | View Issue

Cite this: *Chem. Sci.*, 2020, **11**, 7694

All publication charges for this article have been paid for by the Royal Society of Chemistry

A magnetic solder for assembling bulk covalent adaptable network blocks†

Shuai Zhang,[a] Yubai Zhang,[a] Yahe Wu,[a] Yang Yang,[a] Qiaomei Chen,[a] Huan Liang,[a] Yen Wei*[ab] and Yan Ji*[a]

Received 21st March 2020
Accepted 31st May 2020

DOI: 10.1039/d0sc01678k

rsc.li/chemical-science

Covalent adaptable networks (CANs) represent a novel covalently cross-linked polymer that is capable of being reprocessed and recycled relying on reversible covalent bond structures and present exceptional opportunities in a wide range of prospective applications. However, it is genuinely difficult to fabricate bulk CAN blocks with solid-core geometries that possess complex shapes or multiple materials, which are crucial in cutting-edge fields such as soft robotics, flexible electronic devices and biomedical engineering. Here we report a welding technique to strategically construct complex and heterogeneous 3D CAN structures by utilizing a solder doped with magnetic nanoparticles. The solder is able to induce a bond exchange reaction at the interface between the to-be-welded pieces. Using this method, not only CAN bulks with the same materials can be welded to form complex geometries, distinctive bulks with different physical properties and chemical compositions can also be connected to fabricate multimaterial devices. Besides, this method can be used to repair damaged CAN materials and efficiently recycle scrap CAN materials, which can effectively save resources and protect the environment. The universality and robustness of this strategy is expected to promote CAN application in broader functional polymer fields.

1. Introduction

In the past two decades, polymer science has witnessed the fast blooming of covalent adaptable networks (CANs), which have successfully bridged the distinct gap between traditional thermoplastics and thermosets. Even though CANs are covalently cross-linked like thermosets which are hard to reprocess, they have notable recyclability while maintaining the commendable features of thermosets such as an infusible structure and high mechanical performance.[1–11] They are especially appealing for a sustainable society since an enormous amount of plastic waste has caused immense trouble.[12,13] How to efficiently realize the recycling of CANs relying on bond exchange reactions is of critical importance. Welding technology, as an additive manufacturing method, offers good tactics to reuse CANs, which do not require the reprocessing of the whole material thus maintaining the original properties of the non-welded area, to assemble pieces into new structures or to mend the damaged part with new materials.[14–17] Unlike adhesive bonding or mechanical fastening, welding of CANs based on bond exchange reactions can join CAN pieces at a molecular level, which maintains the union of the obtained CAN materials. Welding also makes it possible to strategically construct heterogeneous 3D structures using covalent bonds, which is impossible for traditional thermosets but significantly affects the application of the materials.[18–21]

However, it is extremely difficult to weld large-sized bulk CAN blocks. Bulk CAN blocks with solid-core geometries have higher tensile strength and excellent anti-cracking capability as well as strong shock resistance ability. They are irreplaceable for traditional industrial applications and are more functional in many frontier applications (*e.g.* soft robotics with powerful actuation force) compared to their film counterparts.[22,23] Assembling bulk CAN blocks into complex 3D structures is of critical importance because the structure of objects often inherently determines their functions.[24,25] The lack of suitable external stimuli to activate bond exchange makes it difficult to weld bulk CAN blocks directly. Current stimuli to induce bond exchange reactions mainly include direct heat and light. Direct heat has distinct advantages as it is compatible with traditional manufacturing processing techniques and it enables CANs to be repurposed for new applications by reshaping or remolding. However, if direct heat is used to weld bulk CAN blocks, it is likely to cause unwanted permanent deformation of the whole material (although this is important for the remodeling of CAN materials, it is not suitable for welding bulk CAN blocks) because a relatively high pressure is often required to ensure

[a]*The Key Laboratory of Bioorganic Phosphorus Chemistry & Chemical Biology (Ministry of Education), Department of Chemistry, Tsinghua University, Beijing 100084, China. E-mail: jiyan@mail.tsinghua.edu.cn; weiyen@tsinghua.edu.cn*

[b]*Department of Chemistry, Center for Nanotechnology, Institute of Biomedical Technology, Chung-Yuan Christian University, Chung-Li 32023, Taiwan, China*

† Electronic supplementary information (ESI) available. See DOI: 10.1039/d0sc01678k

good contact at the interface.[26–31] It is possible to deliver heat to local areas by some traditional methods of soldering. However, limitations such as the introduction of solder impurities and requirement for complex operations have to be considered when these traditional soldering methods are intended to be used for localized heating. As another common stimulus, light is also inapplicable for welding CAN bulks. Although light can be concentrated at the interface without affecting the rest of the parts, the penetration of light is relatively poor which makes welding large bulk materials very difficult.[18,24,32] Therefore, there is an urgent need for a novel external stimulus that can induce bond exchange reactions to realize welding of large-sized bulk CAN blocks.

Here, we propose an effective stimulus to weld large-sized bulk CAN blocks by utilizing a magnetic field. Our strategy is to develop a magnetic-responsive CAN solder which can provide heat due to the widely-known magnetothermal effect.[33–35] Consequently, when exposed to an alternating magnetic field (AMF), bond exchange reactions can be induced (by the magnetothermal effect) at the interface between the solder and the to-be-welded pieces, which results in rapid welding of the large-sized bulk CAN blocks. As a demonstration, we prepared Fe_3O_4 nanoparticle dispersed polyurethane (PU) CANs. The welding is based on transcarbamoylation (a carbamate-only bond exchange reaction) which was found for PU CANs by Xie and co-workers in 2016 and can be thermally initiated in the presence of catalysts (Fig. 1a).[36] PU CANs can undergo complete stress relaxation at 130 °C and have faster relaxation times with higher DBTDL (a common catalyst) contents. This finding suggests that the exchange of carbamate bonds can be realized at 130 °C. We placed a PU CAN solder (film) which contains Fe_3O_4 nanoparticles between the target bulks (or foams) and applied compressive stress to maintain good contact. In the alternating magnetic field, heat is generated by power loss of superparamagnetic Fe_3O_4 nanoparticles,[37] which can be used to trigger transcarbamoylation to realize the interface welding within minutes.

The reason why our method can realize welding of bulk CAN blocks while previous approaches struggled is because of the special properties of magnetic materials.[34,38–45] On the one hand, the magnetothermal effect has a strong penetrating power, which enables welding regardless of the size of the material. On the other hand, the magnetothermal effect only occurs in the part containing magnetic substances keeping the rest of the parts unaffected. Therefore, when the magnetic-nanoparticle-free CAN bulks are welded using a solder, the dynamic exchange reaction only occurs at the interface between the solder and bulks. As a result, this process does not affect the shape and mechanical properties of the "blank" parts.

This welding method has distinct advantages in real-world applications. 3D structures with complex geometries constructed with basic bulk modules can be easily achieved. Compared to 3D structures fabricated with films, 3D bulk structures with solid-core geometries are "stronger" which can offer firmer support and increased flexibility. Not only bulk CAN blocks composed of the same components can be welded, CAN bulks possessing different physical properties or chemical compositions can also be joined together to build multimaterial or multi-functional devices as long as their welding mechanism is based on bond exchange reactions. In addition, this technique also enables the repairing and recycling of bulk CAN blocks after damage and offers possibility for "gluing" together scrap materials, which can reduce waste and effectively improve material recycling compared to remolding. Besides, the solder can act alone as an excellent magnetic-responsive material and achieve shape memory, reshaping and healing, which is promising for a wide range of applications including intelligent implants, aeronautics, biomedicine and flexible electronics.[37,46,47]

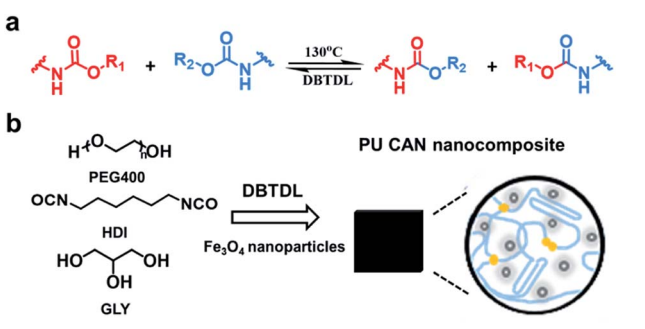

Fig. 1 (a) An illustration of reversible transcarbamoylation. (b) Synthesis of the PU CAN nanocomposite.

2. Results and discussion

2.1. Magnetically controlled performances of the PU CAN solder

2.1.1. Synthesis and characterization of the PU CAN solder.

The magnetic-responsive solder was synthesized by reacting poly(ethylene glycol)diol (M_n = 400) and glycerin with hexamethylene diisocyanate in the presence of dibutyltin dilaurate (DBTDL) as a catalyst for transcarbamoylation (Fig. 1b). Commercial Fe_3O_4 nanoparticles (diameter: 20 nm) were chosen as the dopant to induce the magnetothermal effect because of their excellent properties such as a strong magnetic moment, good biocompatibility and high magnetothermal conversion rates. Superparamagnetic Fe_3O_4 nanoparticles (10 wt%, 20 wt% or 50 wt%) were added into the solution and homogeneously dispersed by vigorous stirring (abbreviated to PU–10% Fe_3O_4, PU–20% Fe_3O_4, and PU–50% Fe_3O_4, respectively). Swelling experiments suggest that all the above samples have high gel contents (97.62%, 98.41%, and 97.49%, respectively), which confirm their thermosetting nature. The overall mechanical and thermal properties were tested, and dynamic mechanical analysis (DMA) (Fig. 2a) shows that all the samples with various Fe_3O_4 nanoparticle contents undergo complete stress relaxation at 130 °C, which indicates that the addition of Fe_3O_4 nanoparticles has little effect on transcarbamoylation. According to differential scanning calorimetry (DSC) curves (Fig. S1†), the glass transition temperatures (T_g) of the Fe_3O_4–PUs are about −17 °C, which is slightly lower than the T_g of the control PU material (−15 °C). Since the degradation

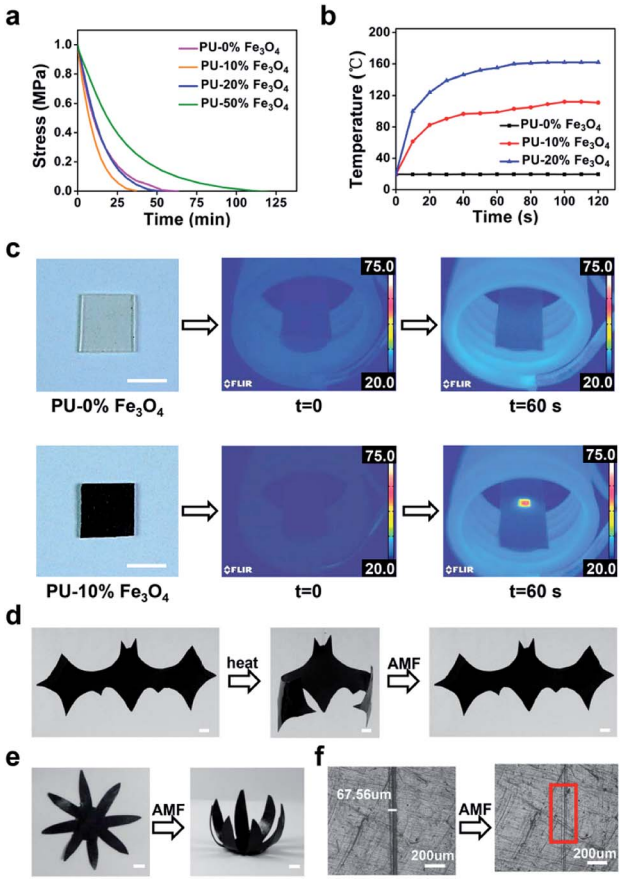

Fig. 2 (a) Stress relaxation behaviours of PUs with different Fe_3O_4 nanoparticle contents at 130 °C. (b) Heating curves of PUs with different Fe_3O_4 nanoparticle contents under the same experimental conditions. (c) Infrared images of PUs with the same volume and without Fe_3O_4 and with Fe_3O_4-10 wt% in the same alternating magnetic field. (d) Illustration of magnetothermal effect induced shape memory of PU–10% Fe_3O_4. (e) Reshaping due to the magnetothermal effect induced transcarbamoylation. (f) Magnetothermal effect triggered healing of PU–10% Fe_3O_4 in the alternating magnetic field.

temperature of all the samples is above 270 °C as measured by thermogravimetric analysis (TGA), the addition of Fe_3O_4 nanoparticles does not affect the stability of the nanocomposites (Fig. S2†). Stress–strain curves confirm that the incorporation of Fe_3O_4 nanoparticles has little effect on the mechanical properties of the materials at room temperature (25 °C) (Fig. S3†).

More importantly, these nanocomposites demonstrate excellent magnetically responsive characteristics in the AMF. Under the conditions of the same frequency and electricity, a certain volume of PU with more Fe_3O_4 nanoparticles dispersed in the polymer matrix could reach higher temperature faster in a certain time period (the temperature of samples was observed with a thermographic camera) (Fig. 2b). Control experiments were also performed to testify the magnetothermal effect of PU solders (Fig. 2c). The temperature of PU–10% Fe_3O_4 (5.75 mm × 5.75 mm × 0.40 mm) could reach 68 °C in 60 s (f = 320 kHz, H = 198.489 Gs), while the control sample (the same volume) without Fe_3O_4 nanoparticles showed a negligible change (<1 °C).

2.1.2. Magnetically controlled shape memory, reshaping and healing of the PU CAN solder. The commendable magnetothermal effect of the nanocomposites enables efficient shape memory, reshaping and healing in the AMF. As shown in Fig. 2d, PU–10% Fe_3O_4 (T_g is about 18 °C) was used to make a mimetic bat. The wings of the "bat" were bent at 60 °C (above T_g) and then directly cooled to room temperature (about 5 °C) to fix the temporary shape. Afterwards, the folded bat was placed in the AMF (f = 320 kHz, H = 198.489 Gs) and its wings unfolded to its permanent shape when the temperature was higher than T_g. The permanent shape of this nanocomposite can also be changed by using the magnetothermal effect to induce transcarbamoylation. Fig. 2e shows that an 8-petal flower (PU–10% Fe_3O_4) was bent and fixed with tapes, which was placed in the AMF (f = 320 kHz, H = 198.489 Gs) for 5 min and the apparent temperature of the flower was around 140 °C. The flower was then cooled down to room temperature. After removing the tapes, we found that the petals stayed curved. Without any external force intervention, the flower with curved petals could maintain its shape when heated to 140 °C for 20 min, which suggests that the transformation from a 2D shape to 3D shape is successfully realized. However, in the control experiment, it took about 20 min with direct heating to change the permanent shape of the same material. This is because the heat-producing Fe_3O_4 nanoparticles inside the polymer reduces the heat loss caused by heat transfer and thermal diffusion, which improves the efficiency of transcarbamoylation. Moreover, this nanocomposite has valuable healing properties due to the magnetothermal effect induced transcarbamoylation. Fig. 2f shows PU–10% Fe_3O_4 was cut with a razor to form a 70 μm seam. This damaged cut was healed effectively after the sample was placed in the AMF (f = 495 kHz, H = 166.787 Gs) for 2 min. Such *in situ* healing is useful to improve the long-term device maintenance.

2.1.3. Magnetically controlled welding of the PU CAN solder. In addition to the above multiple functions, more importantly, this nanocomposite enables robust welding under

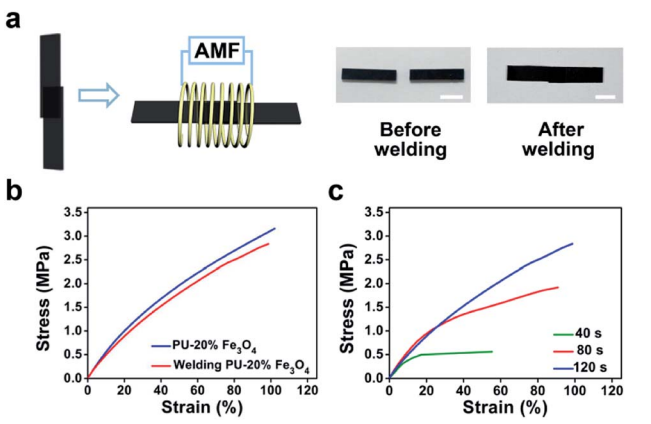

Fig. 3 (a) Illustration of the magnetothermal effect induced welding of PU–20% Fe_3O_4. (b) Lap-shear tests of the controlled sample and welded PU–20% Fe_3O_4. (c) Effect of the welding time on joint results. For the samples which were irradiated for 40 s and 80 s, the stress at break was 0.5 MPa and 1.8 MPa, respectively, and the two films separated in the overlap regions.

the AMF. Fig. 3a shows that two films (PU–20% Fe_3O_4) are pressed together with an overlap area of 3.0 mm × 3.0 mm. After placing the sample in the alternating magnetic field for 2 min, transcarbamoylation was activated and the welding was completed. Lap-shear tests were carried out to further investigate the welding efficiency. The welded sample had almost the same mechanical properties as the blank sample; the welded film broke in the regions of bulk materials instead of the overlapped part, which again indicates a strong joint realized by transcarbamoylation (Fig. 3b). The effect of the welding time was also investigated and 2 min was selected as the optimal condition (Fig. 3c).

2.2. Magnetically controlled welding of bulk CAN blocks

2.2.1. Welding PU CAN bulks and foams by using the magnetic-responsive solder. Bulk CAN blocks with solid-core geometries which possess complex shapes or multiple materials are crucial in cutting-edge fields. However, CAN bulks (including foams) are extremely difficult to weld by using current stimuli such as light and direct heat. The penetration of light is relatively poor which makes welding of large bulk materials very difficult. Welding by direct heat is difficult to use in assembling CAN bulks because the overall shape of the material would suffer from deformation under pressure which is essential to maintain good interface contact. Of course, some traditional methods of soldering can deliver heat to local areas, like wire soldering or hot-tool welding (thermal welding for joining thermoplastic composites). However, the mechanical properties of solders (wire solders are always metal materials) are quite different from the those of the original CAN materials, which significantly affects the application of the combined objects. For the hot-tool welding technique, the hot-tool is clamped between the welded interfaces to heat the objects and then removed to achieve welding in the presence of applied pressure, which is not suitable for large-sized welded parts and precise temperature control.[48] Fig. 4a shows that the two PU CAN bulks were directly heated to 140 °C for 20 min (the most commonly used method for welding CAN films). Although the two PU CAN bulks were welded together, their shape was severely deformed and became yellow. Similarly, the PU CAN foams could be welded together, but at the expense of severe yellowing. This is because the dynamic exchange reaction occurs in the whole material causing deformation under external pressure and the entire material is easily oxidized at high temperature. The best solution is to maintain the shape and mechanical properties of the non-welded parts simultaneously achieving satisfactory interfacial bonding.

Considering that the magnetothermal effect only occurs in areas containing magnetic substances, we utilize Fe_3O_4-nanoparticle-doped films as solders to weld PU CAN bulks. As a demonstration (Fig. 4b), we placed a solder (PU–50% Fe_3O_4) between the two PU bulks and tied them with PTFE tape to maintain good contact. Then the sample was heated to 150 °C for 1 min in the AMF (f = 495 kHz, H = 127.331 Gs). After cooling the bulks to room temperature, the material was successfully welded. To prove that the welding was successful,

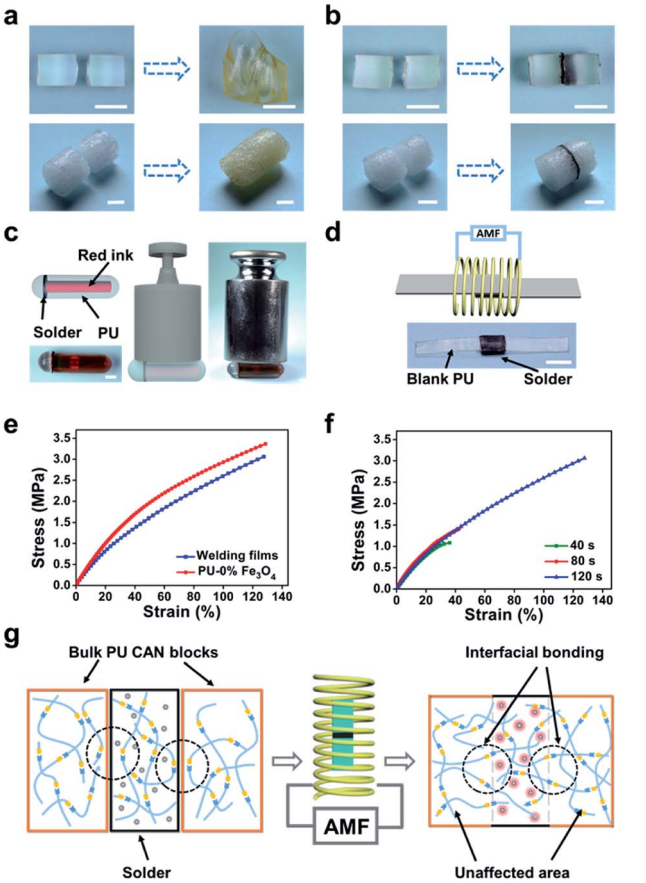

Fig. 4 (a) Welding of PU CAN bulks and foams by direct heating at 140 °C for 20 min. (b) Welding of PU bulks and foams by using a magnetothermal responsive solder in the alternating magnetic field. (c) Poured red ink into the PU tube, sealed and pressed with a weight of 500 grams for two days. (d) A thin layer of PU–50% Fe_3O_4 was sandwiched between two PU films and the films were placed in the alternating magnetic field. (e) Lap-shear tests of the welded film and the control sample. (f) Effect of the welding time on joint results. (g) The mechanism of the magnetothermal effect to weld PU CAN bulks.

swelling experiments were conducted in ethyl acetate (EA) at 40 °C for 48 h. After swelling and drying, the sample was still welded, which indicates that the joining of the two bulks is very good. Another visual demonstration was made to testify the success of welding bulk CAN blocks. As shown in Fig. 4c, we made a hollow tube with one side open and put red ink in it. We used the welding method to seal the open side. After that, we applied a weight of 500 grams to the pipe and two days later, the joint remained intact without liquid leaking out. As observed in the ESI, a microscope was used to observe the cross-sectional area of the welded sample (Fig. S4†). It was obvious that both the external area and internal area of the bulk PU CAN blocks are successfully welded.

To further characterize the welding efficiency, a thin layer of PU–50% Fe_3O_4 was sandwiched between two PU CAN films, and the two pieces of PU could be joined together by being placed in the AMF (Fig. 4d). The lap-shear test (Fig. 4e) shows that the welded film breaks at the blank part, which means that the solder could weld bulk PU CAN blocks.

Similarly, we studied the effect of the welding time (Fig. 4f). The optimum time was 2 min when the size of the solder is 3.5 mm × 4.5 mm × 0.4 mm. Visual interpretation is shown in Fig. 4g. When the bulk CAN blocks and the solder are placed in the AMF, the Fe_3O_4-nanoparticle-doped solder will be heated quickly because of the magnetothermal effect. Due to heat transfer, the contact surfaces of the solder and the bulks will be heated to a relatively high temperature (about 140 °C) to trigger the bond exchange reaction, while the temperature in other parts of the material remains unchanged, which ensures the stability of the shape and mechanical properties of the bulk materials.

Moreover, using the "building blocks" approach, 3D macro bulk materials (including foams) can be easily obtained by separately preparing simple modules and then "gluing" them together. For example, Fig. 5a shows an assembled "plane" fabricated *via* first making separate simple bulk materials such as cubes, cuboids and cylinders and then welding them together by placing solders between each bulk and placing the bulks in the AMF. The operation was very simple and conducted in a very short time, while the direct preparation of such a complex plane-like material generally requires complicated molds or an intricate procedure for material reduction. Meanwhile, the solder can be cut from the welded materials and repeatedly used for welding other PU materials, which contributes to protecting the environment. PU foam is also a very important kind of bulk material; In particular smart foams are widely used in drug delivery systems, biosensors and aerospace devices.[49–51] Assembly of foams with different properties and complex structures is of great significance for the preparation of advanced devices. As a demonstration, we easily achieved the welding of cylindrical foams (Fig. 5b), which shows the great application potential of this method in welding and repairing foam materials (Fig. S5†).

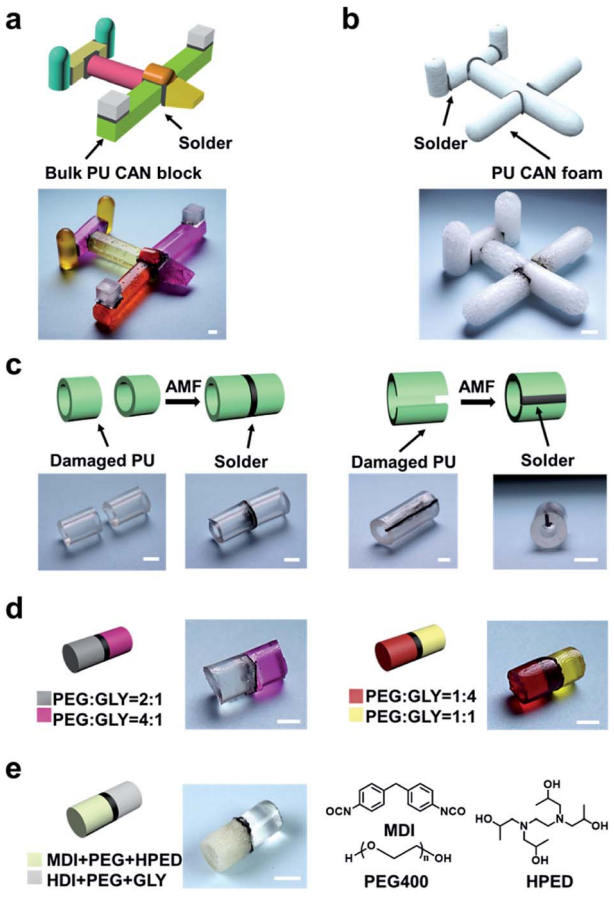

Fig. 5 (a) The assembled complex plane-like PU CAN bulk. (b) Assembled complex plane-like PU CAN foam. (c) Repaired PU CAN tubes with this welding technology. (d) Joined PU CAN bulks with different physical properties. (e) Joined PU CAN bulks with different chemical components and the chemical components of PU-5.

2.2.2. Repairing PU CAN bulks by using the magnetic-responsive solder. Repairing of bulk materials can also be robustly realized. As shown in Fig. 5c, we could easily repair a PU CAN tube with this welding technology. The solder was placed in the crack and a certain external force was applied to keep the interface in good contact. Then we placed the tube in the AMF ($f = 495$ kHz, $H = 127.331$ Gs) and heated to 140 °C for 1 min. When the composite was cooled down to room temperature, a complete tube was obtained. Specifically, we can prepare welding solders withf similar mechanical properties according to targeted materials. The consistency of the mechanical properties of the original materials can be maintained whether the materials are assembled into complex-shaped devices or being repaired.

2.2.3. Welding PU CAN bulks that possess different physical properties and chemical components. Not only CAN bulks with the same chemical composition can be joined together, but bulk CAN blocks with different physical properties and chemical components can also be efficiently welded. These experiments explored the carbamate bond exchange reaction between PU CANs with different chemical components. We prepared 4 PU-cylinders (Fig. 5d) with different physical properties, named PU-1 (achromatous), PU-2 (pink), PU-3 (red) and PU-4 (yellow). These cylinders were synthesized by changing the cross-linking density which results in different rigidity. Welding of PU-1 and PU-2 or PU-3 and PU-4 can create complex PU CAN bulk structures with heterogeneous stiffness which is essentially required in material assembly. More importantly, PU CAN bulks with completely different chemical components can be welded together. PU-5 (white) was fabricated by changing HDI to MDI and the cross-linker was changed from GLY to HPED. Welding of PU-1 and PU-5 by using the magnetic-responsive solder (Fig. 5e) suggests that this solder enables CAN to weld regardless of the chemical components of PUs. The invention of this solder makes welding of bulk CAN blocks with different chemical components and physical properties possible to endow the composites with multiple functions which can substantially benefit their application in soft robotics.

3. Conclusions

In summary, we show here that bulk CAN blocks can be efficiently welded together using an appropriately designed magnetic solder. The special feature of the magnetic field allows the bond exchange reaction only to occur at the interface

between the solder and CAN bulks while keeping the shape and mechanical properties of the non-welded parts unaffected. Not only bulk CAN blocks of different chemical compositions can be welded together, but damaged CAN bulks and scrap CAN materials can also be efficiently repaired and recycled. Additionally, the compositions and properties of the solder can be flexibly adjusted according to targeted materials, so that the properties of the joint are consistent with those of the original, which will endow composites with better mechanical and thermal properties than using adhesives. The solder can be cut from the welded materials and repeatedly used for welding other CAN materials which can be considered as resource saving. This strategy can be further generalized to multiple systems and has the potential to be applied in cutting-edge functional polymer fields including soft robotics, aeronautics, flexible electronic devices and biomedical engineering to satisfy the needs of practical applications.

Conflicts of interest

There are no conflicts to declare.

Acknowledgements

This research was supported by the National Natural Science Foundation of China (no. 51722303, 21674057 and 21788102).

Notes and references

1 C. J. Kloxin and C. N. Bowman, *Chem. Soc. Rev.*, 2013, **42**, 7161–7173.
2 C. N. Bowman and C. J. Kloxin, *Angew. Chem., Int. Ed.*, 2012, **51**, 4272–4274.
3 C. J. Kloxin, T. F. Scott, B. J. Adzima and C. N. Bowman, *Macromolecules*, 2010, **43**, 2643–2653.
4 M. K. McBride, B. T. Worrell, T. Brown, L. M. Cox, N. Sowan, C. Wang, M. Podgorski, A. M. Martinez and C. N. Bowman, *Annu. Rev. Chem. Biomol. Eng.*, 2019, **10**, 175–198.
5 Y. Heo and H. A. Sodano, *Adv. Funct. Mater.*, 2014, **24**, 5261–5268.
6 X. Chen, M. A. Dam, K. Ono, A. Mal, H. Shen, S. R. Nutt, K. Sheran and F. Wudl, *Science*, 2002, **295**, 1698–1702.
7 S. J. Rowan, S. J. Cantrill, G. R. Cousins, J. K. Sanders and J. F. Stoddart, *Angew. Chem., Int. Ed.*, 2002, **41**, 898–952.
8 R. J. Wojtecki, M. A. Meador and S. J. Rowan, *Nat. Mater.*, 2011, **10**, 14.
9 Y. Jin, Q. Wang, P. Taynton and W. Zhang, *Acc. Chem. Res.*, 2014, **47**, 1575–1586.
10 D. Montarnal, M. Capelot, F. Tournilhac and L. Leibler, *Science*, 2011, **334**, 965–968.
11 Y. Jin, Z. Lei, P. Taynton, S. Huang and W. Zhang, *Matter*, 2019, **1**, 1456.
12 W. Zou, J. Dong, Y. Luo, Q. Zhao and T. Xie, *Adv. Mater.*, 2017, **29**, 1606100.
13 P. Zhang and G. Li, *Prog. Polym. Sci.*, 2016, **57**, 32–63.
14 M. Capelot, D. Montarnal, F. Tournilhac and L. Leibler, *J. Am. Chem. Soc.*, 2012, **134**, 7664–7667.
15 K. Yu, Q. Shi, H. Li, J. Jabour, H. Yang, M. L. Dunn, T. Wang and H. J. Qi, *J. Mech. Phys. Solids*, 2016, **94**, 1–17.
16 C. B. Sweeney, B. A. Lackey, M. J. Pospisil, T. C. Achee, V. K. Hicks, A. G. Moran, B. R. Teipel, M. A. Saed and M. J. Green, *Sci. Adv.*, 2017, **3**, e1700262.
17 Y. Amamoto, J. Kamada, H. Otsuka, A. Takahara and K. Matyjaszewski, *Angew. Chem., Int. Ed.*, 2011, **50**, 1660–1663.
18 Z. Pei, Y. Yang, Q. Chen, Y. Wei and Y. Ji, *Adv. Mater.*, 2016, **28**, 156–160.
19 M. A. C. Stuart, W. T. Huck, J. Genzer, M. Müller, C. Ober, M. Stamm, G. B. Sukhorukov, I. Szleifer, V. V. Tsukruk and M. Urban, *Nat. Mater.*, 2010, **9**, 101.
20 W. Li, X. Liu, Z. Deng, Y. Chen, Q. Yu, W. Tang, T. L. Sun, Y. S. Zhang and K. Yue, *Adv. Mater.*, 2019, 1904732.
21 Y. Zhang, Z. Wang, Y. Yang, Q. Chen, X. Qian, Y. Wu, H. Liang, Y. Xu, Y. Wei and Y. Ji, *Sci. Adv.*, 2020, **6**, eaay8606.
22 B. Jin, H. Song, R. Jiang, J. Song, Q. Zhao and T. Xie, *Sci. Adv.*, 2018, **4**, eaao3865.
23 A. Lendlein, M. Behl, B. Hiebl and C. Wischke, *Expert Rev. Med. Devices*, 2010, **7**, 357–379.
24 Y. Yang, Z. Pei, Z. Li, Y. Wei and Y. Ji, *J. Am. Chem. Soc.*, 2016, **138**, 2118–2121.
25 C. Ma, T. Li, Q. Zhao, X. Yang, J. Wu, Y. Luo and T. Xie, *Adv. Mater.*, 2014, **26**, 5665–5669.
26 Z. Pei, Y. Yang, Q. Chen, E. M. Terentjev, Y. Wei and Y. Ji, *Nat. Mater.*, 2014, **13**, 36.
27 P. Taynton, H. Ni, C. Zhu, K. Yu, S. Loob, Y. Jin, H. J. Qi and W. Zhang, *Adv. Mater.*, 2016, **28**, 2904–2909.
28 A. R. de Luzuriaga, R. Martin, N. Markaide, A. Rekondo, G. Cabañero, J. Rodríguez and I. Odriozola, *Mater. Horiz.*, 2016, **3**, 241–247.
29 W. Denissen, G. Rivero, R. Nicolaÿ, L. Leibler, J. M. Winne and F. E. Du Prez, *Adv. Funct. Mater.*, 2015, **25**, 2451–2457.
30 H. Xiang, H. Qian, Z. Lu, M. Rong and M. Zhang, *Green Chem.*, 2015, **17**, 4315–4325.
31 Z. Q. Lei, P. Xie, M. Z. Rong and M. Q. Zhang, *J. Mater. Chem. A*, 2015, **3**, 19662–19668.
32 Z. Li, Y. Yang, Z. Wang, X. Zhang, Q. Chen, X. Qian, N. Liu, Y. Wei and Y. Ji, *J. Mater. Chem. A*, 2017, **5**, 6740–6746.
33 K. Hu, J. Sun, Z. Guo, P. Wang, Q. Chen, M. Ma and N. Gu, *Adv. Mater.*, 2015, **27**, 2507–2514.
34 R. Mohr, K. Kratz, T. Weigel, M. Lucka-Gabor, M. Moneke and A. Lendlein, *Proc. Natl. Acad. Sci. U. S. A.*, 2006, **103**, 3540–3545.
35 J. Tang, Z. Tong, Y. Xia, M. Liu, Z. Lv, Y. Gao, T. Lu, S. Xie, Y. Pei and D. Fang, *J. Mater. Chem. B*, 2018, **6**, 2713–2722.
36 N. Zheng, Z. Fang, W. Zou, Q. Zhao and T. Xie, *Angew. Chem., Int. Ed.*, 2016, **55**, 11421–11425.
37 Y. Cai, J. S. Jiang, B. Zheng and M. R. Xie, *J. Appl. Polym. Sci.*, 2013, **127**, 49–56.
38 J. Thévenot, H. Oliveira, O. Sandre and S. Lecommandoux, *Chem. Soc. Rev.*, 2013, **42**, 7099–7116.
39 A. M. Schmidt, *Macromol. Rapid Commun.*, 2006, **27**, 1168–1172.
40 Q. A. Pankhurst, J. Connolly, S. K. Jones and J. Dobson, *J. Phys. D: Appl. Phys.*, 2003, **36**, R167.

41 J.-H. Lee, J.-t. Jang, J.-s. Choi, S. H. Moon, S.-h. Noh, J.-w. Kim, J.-G. Kim, I.-S. Kim, K. I. Park and J. Cheon, *Nat. Nanotechnol.*, 2011, **6**, 418.
42 N. A. Frey, S. Peng, K. Cheng and S. Sun, *Chem. Soc. Rev.*, 2009, **38**, 2532–2542.
43 H. Zeng and S. Sun, *Adv. Funct. Mater.*, 2008, **18**, 391–400.
44 W. Hu, G. Z. Lum, M. Mastrangeli and M. Sitti, *Nature*, 2018, **554**, 81–85.
45 Y. Kim, H. Yuk, R. Zhao, S. A. Chester and X. Zhao, *Nature*, 2018, **558**, 274–279.
46 X. Zhao, J. Kim, C. A. Cezar, N. Huebsch, K. Lee, K. Bouhadir and D. J. Mooney, *Proc. Natl. Acad. Sci. U. S. A.*, 2011, **108**, 67–72.
47 P. R. Buckley, G. H. McKinley, T. S. Wilson, W. Small, W. J. Benett, J. P. Bearinger, M. W. McElfresh and D. J. Maitland, *IEEE Trans. Biomed. Eng.*, 2006, **53**, 2075–2083.
48 A. Yousefpour, M. Hojjati and J.-P. Immarigeon, *J. Thermoplast. Compos. Mater.*, 2004, **17**, 303–341.
49 X. Cao, L. J. Lee, T. Widya and C. Macosko, *Polymer*, 2005, **46**, 775–783.
50 F. Quadrini, D. Bellisario and L. Santo, *Polym. Eng. Sci.*, 2013, **53**, 1357–1363.
51 K. H. Choe, D. S. Lee, W. J. Seo and W. N. Kim, *Polym. J.*, 2004, **36**, 368.